Manifold learning for coherent design interpolation based on geometrical and topological descriptors

D. Muñoz, O. Allix, Francisco Chinesta, J.J. Ródenas, E. Nadal

Available online at www.sciencedirect.com
ScienceDirect
Comput. Methods Appl. Mech. Engrg. 405 (2023) 115859
Computer methods in applied mechanics and engineering
www.elsevier.com/locate/cma

Manifold learning for coherent design interpolation based on geometrical and topological descriptors

D. Muñoz[a,c,*], O. Allix[b], F. Chinesta[c], J.J. Ródenas[a], E. Nadal[a]

[a] *Institute of Mechanical and Biomechanical Engineering (I2MB), Universitat Politècnica de València, Building 5E, Camino de Vera s/n, 46022 Valencia, Spain*
[b] *Université Paris-Saclay, ENS Paris-Saclay, CentraleSupélec, CNRS, LMPS - Laboratoire de Mécanique Paris-Saclay, 91190, Gif-sur-Yvette, France*
[c] *ESI Chair, PIMM, Arts et Métiers Institute of Technology, 151 Boulevard de l'Hopital, F-75013 Paris, France*

Received 29 September 2022; received in revised form 15 December 2022; accepted 15 December 2022
Available online 12 January 2023

Abstract

In the context of intellectual property in the manufacturing industry, know-how is referred to practical knowledge on how to accomplish a specific task. This know-how is often difficult to be synthesised in a set of rules or steps as it remains in the intuition and expertise of engineers, designers, and other professionals. Today, a new research line in this concern spot-up thanks to the explosion of Artificial Intelligence and Machine Learning algorithms and its alliance with Computational Mechanics and Optimisation tools. However, a key aspect with industrial design is the scarcity of available data, making it problematic to rely on deep-learning approaches. Assuming that the existing designs live in a manifold, in this paper, we propose a synergistic use of existing Machine Learning tools to infer a reduced manifold from the existing limited set of designs and, then, to use it to interpolate between the individuals, working as a generator basis, to create new and coherent designs. For this, a key aspect is to be able to properly interpolate in the reduced manifold, which requires a proper clustering of the individuals. From our experience, due to the scarcity of data, adding topological descriptors to geometrical ones considerably improves the quality of the clustering. Thus, a distance, mixing topology and geometry is proposed. This distance is used both, for the clustering and for the interpolation. For the interpolation, relying on optimal transport appear to be mandatory. Examples of growing complexity are proposed to illustrate the goodness of the method.

Keywords: Structural optimisation; Machine learning; Dimensionality reduction; Locally linear embedding; Topological data analysis; Optimal transport

1. Introduction

In the context of intellectual property in the industry, know-how is referred to the practical knowledge about how to accomplish a specific task [1]. Most of this know-how resides in the intuition and expertise of engineers and designers, among a wide variety of professionals. Thus, it is extremely difficult to characterise by rules or steps. In order to not lose a given know-how, we would like to be able to extract it from the objects previously created.

* Corresponding author.
E-mail addresses: damuopel@upv.es (D. Muñoz), olivier.allix@ens-paris-saclay.fr (O. Allix), francisco.chinesta@ensam.eu (F. Chinesta), jjrodena@mcm.upv.es (J.J. Ródenas), ennaso@upvnet.upv.es (E. Nadal).

https://doi.org/10.1016/j.cma.2022.115859

For this, as it is done today in many other domains in engineering, we propose to ally tools emerging from Artificial Intelligence and Machine learning with techniques belonging to Computational Mechanics and Optimisation. But what could be a possible strategy? A key difficulty is scarcity in the number of designs in a given industry. This implies that it is not possible to properly use deep-learning approaches for this purpose [2]. Therefore, among the available tools, we have selected those allowing us to infer, if possible, a reduced manifold of the existing designs. Being its existence our main hypothesis. It will be possible if these techniques can adequately approximate the low dimensionality space where the current designs belong to. This is mandatory because, with few individuals, compared to deep-learning approaches, one can expect to interpolate, in a sense to be precised later, only in low dimensional space.

In our scientific context, a related question naturally arises: how to characterise the existing component designs? This first paper will consider the design as the objects' geometries. Clearly, in the future, we should include other characterisations, as the strains or stress fields, for instance, two crucial measures in the structural mechanics field. Even considering this restricted definition of design, one should be precise in characterising a geometry because there exist multiple ways to do it. In fact, it is our experience that this choice may significantly influence the dimensions of the reduced manifold. A criterion of choice is that the implicit space should be a manifold of possible designs. That is, we need to create appropriate designs when interpolating between existing designs.

The first part of the paper is devoted to finding a shape characterisation that allows obtaining an attractive latent space of existing designs and interpolating in this reduced space. The designs are characterised by their geometry and topology. The relevance of the geometrical information is evident. However, in the context of small data, topology play an important role since it is additional information than the algorithms may use. Among those descriptors, the easiest to manipulate are those based on fields. Thus, for the geometry, we employ the Level-set Functions [3,4]. For the topology we use the principle of persistent homology [5], which belongs to the field of Topological Data Analysis tools [6,7], to create a geometrical 2D image of the topology of the object, the so-called persistence image [8]. Mixing geometrical and topological descriptors is thus possible. Then, we adopt the use of Manifold Learning techniques (ML) [9] to reduce the dimension of the data by extracting the latent structure stored in it. There exists an immense variety of techniques in the ML field, such as the Principal Component Analysis (PCA) [9], which finds the direction of maximum variation in the original dataset. To overcome the limit of this linear technique, non-linear extensions have been proposed. These techniques can preserve the non-linear nature of the original dataset. Among the different non-linear techniques such as Sammon mapping [10], k-PCA [11], Laplacian eigenmaps [12], Isomaps [13] and Autoencoders [14–16], we select the Locally Linear Embedding (LLE) [17]. This technique has been successfully used when data is highly non-linear [18], as in the case of the information coming from the component's topology, and has shown good results in previous works [19,20].

The second part of the paper is devoted to the interpolation of objects in the manifold of the existing designs. Apart from dimensionality reduction, rather than using the entire basis, LLE identifies the neighbours used to reconstruct an individual decreasing the computational cost. The evaluation of the vicinity needed for LLE is usually made employing the distances between individuals, which, in the standard LLE implementation, corresponds to the L_2 euclidean metric. As the scarcity of data is a usual situation in the context we work on, relying on the euclidean norm and the linear interpolation as a basis for the component generator could be ineffective and could also produce components with no physical sense and artefacts. Then, we propose to make use of Optimal Transportation tools (OT) [21–24], which include the Wasserstein metric [22,23]. Additionally, we will consider this metric in the solution of the barycentre problem [25] to interpolate within the objects based on the vicinities defined by the LLE. As a reminder, solving the search of the barycentre problem considering the L_2 euclidean metric is equivalent of using the linear interpolation.

The outline of this article is established as follows. We intend to illustrate the basic ideas with a simple example in each section before applying them to a more complex numerical example of a car bumper. Then, we first try the standard procedure with the LLE algorithm, and in the following sections, we assess the improvements achieved when applying the techniques presented in this introduction. Later, we employ the selected strategy in the car bumper example. To finalise, we conclude the article by gathering some final thoughts.

2. Methodology

Fig. 1 represents the main steps of the methodology presented. In summary, the main goal of this work is to define an interpolation procedure between existing components living in a common manifold. The procedure has

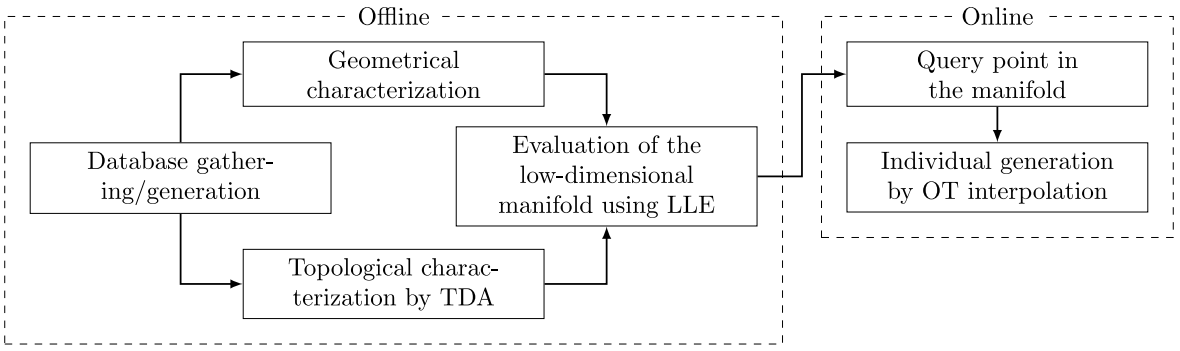

Fig. 1. Simplified workflow of the methodology proposed.

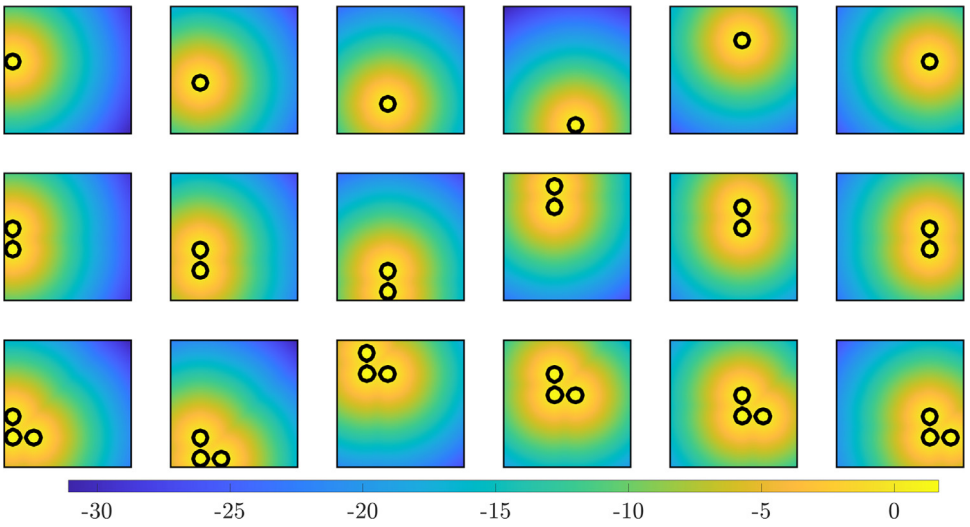

Fig. 2. Signed Distance Function of a representative sampling of the complete database (75 individuals).

an offline and an online phase. The offline phase refers to gathering the dataset and the subsequent treatment that generates the reduced manifold, while the online phase involves the navigation within the manifold and the creation of new components through the interpolation scheme.

2.1. Reference database

We will apply each of the strategies considered in this paper to an elementary academic problem. It consists of a dataset of 75 individuals, the geometry being a square including one, two and three holes, preserving the local shape, but modifying the position. Therefore, the geometry is defined with only 3 parameters: the horizontal position, the vertical position and the number of holes. The reference database is composed of the shape descriptors of each individual. In the introduction, we suggested that geometry descriptors based on domain fields are more convenient for our purpose. Thus, for the geometrical characterisation, we rely on the Level-set method [3,4]. Among the variety of level-set functions available in the bibliography, we employ the Signed Distance Function (SDF), which has the particularity of storing the distance to the boundary of the component. Therefore, the zero-isovalue of the level-set function corresponds to the boundary of the component [26–31]. In this example, each level-set function is discretised by 961 nodes. A subset of the database is shown in Fig. 2. In this Figure, as in the rest of the paper, the geometry of each individual is defined by its SDF.

2.2. Geometry-based strategy

Following the steps illustrated in the workflow scheme, see Fig. 1, the database is gathered and represented in Fig. 2. As we mentioned above, we consider an elementary academic example to describe the proposed strategy. In Fig. 2, we show a sampling of the 75 individuals that compose the database. Each of the individuals is defined by its Signed Distance Function whose zero level (black contour in the images) represents their geometry. Each individual of the database consists of a set of circles of constant diameter that can be located at any position in a square domain. In the standard implementation of the strategy, no further preprocessing of the data is needed, that is, the topological characterisation (step 3 in Fig. 1) is not applied. Then, the next step is to reduce the dimensionality of the database. As we expect the manifold to be of a non-linear nature, we rely here on the Locally Linear Embedding (LLE) algorithm. We chose the LLE algorithm since it provides not only the manifold but a set of non-linear modes that could be used to move into the manifold.

2.2.1. Overview of the original LLE algorithm

Let $\mathbf{X}_i$ be each sample of the training set in the high-dimensional space. The LLE algorithm hypothesise that any point in the database must be obtained as a weighted linear combination of k neighbours with w_{ij}, $j \in [1, k]$ as,

$$\mathbf{X}_i = \sum_j^k w_{ij}\mathbf{X}_j, \tag{1}$$

The neighbours that compose the vicinity of each individual are obtained by choosing the k individuals with smallest distance d_{ij}, evaluated as,

$$d_{ij} = \|\mathbf{X}_i - \mathbf{X}_j\| \tag{2}$$

where $\|\cdot\|$ is the Frobenius norm.

The number of neighbours k is user-defined, and the weights w_{ij} are obtained by minimising the functional represented in Eq. (3):

$$\varepsilon(\mathbf{w}) = \sum_i \|\mathbf{X}_i - \sum_j^k w_{ij}\mathbf{X}_j\|^2, \tag{3}$$

where w_{ij} are subjected to the constraint $\sum_j w_{ij} = 1$. The LLE entrust that these weights are invariant to space transformations. Hence the value of the weights is preserved when changing between spaces. Keeping the weights unchanged, the projection of $\mathbf{X}_i$ on the reduced space, denoted $\mathbf{Y}_i$ is defined by the minimisation of the functional in (4):

$$\epsilon(\mathbf{Y}) = \sum_i \|\mathbf{Y}_i - \sum_j^k w_{ij}\mathbf{Y}_j\|^2, \tag{4}$$

If all eigenvectors are kept, all the original information is stored, otherwise, we retain the eigenvectors associated to the d smallest eigenvalues and maintain the latent structure of the database. The number of eigenvalues is defined by the user and it is assumed to be small. In the reference example, if the technique succeed, it will be 3.

High-dimensional individuals may be obtained as a weighted linear combination of k neighbours, therefore, the reduced manifold of existing designs may be defined as the set of points $\mathbf{Y}$ such that:

$$\mathbf{Y} = \left\{ \sum_j^k \bar{w}_{ij}\mathbf{Y}_j \in \mathbb{R}^d \quad | \quad \sum_j^k \bar{w}_{ij} = 1 \right\} \tag{5}$$

Even though this set is never constructed, an element $\bar{\mathbf{Y}}_i$ in $\mathbf{Y}$ may be associated to the element $\bar{\mathbf{X}}_i$ of the original space as,

$$\bar{\mathbf{X}}_i = \sum_j^k \bar{w}_{ij}\mathbf{X}_j, \tag{6}$$

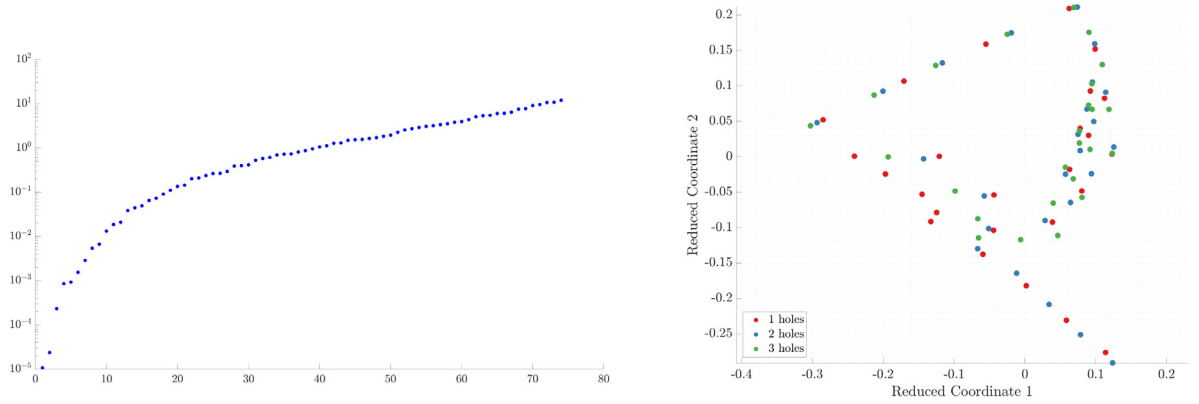

(a) Eigenvalues obtained from minimizing (4). (b) Two first coordinates of the reduced latent space.

Fig. 3. Resulting eigenvalue distribution (a) and reduced coordinates (b) by using the LLE technique with the original data.

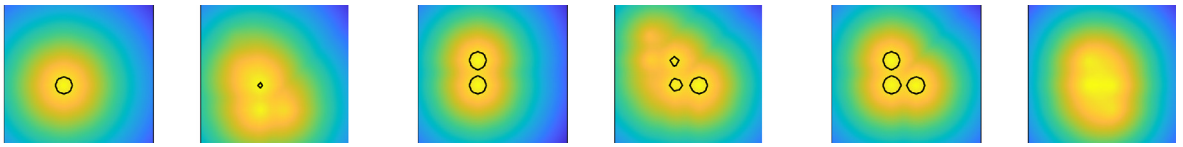

(a) Original component with one hole (left) and the recovered one (right).

(b) Original component with two holes (left) and the recovered one (right).

(c) Original component with three holes (left) and the recovered one (right).

Fig. 4. Examples of original components removed from the database and the recovered ones by the vicinity information.

where the weights $\bar{w}_{ij}$ are obtained by minimising the following functional:

$$\bar{\epsilon}(\bar{\mathbf{w}}) = \|\bar{\mathbf{Y}}_i - \sum_j^k \bar{w}_{ij}\mathbf{Y}_j\|^2. \tag{7}$$

When seeking for a new individual, for example in order to optimise a product, one may search for the best element within the manifold. The technique to perform such a search will be the object of a companion paper.

2.2.2. *Application of the LLE to reference database: results and drawbacks*

We apply here the LLE algorithm to the reference database with the number of neighbours in the vicinity taken as $k = 4$. The resulting eigenvalues are represented in Fig. 3(a) while, in Fig. 3(b), we illustrate the spatial distribution of the coordinates in the reduced space, where each individual is classified by its topology, that is, the number of holes is represented by the colour of the points.

On Fig. 3(a) the eigenvalue spectrum of the problem in (4) is displayed. On this graph the 2 lowest eigenvalues are separated from the rest of the spectrum. This information is used to retain a latent space of dimension 2. In this case, we know beforehand that the reduced space is of dimension 3 (horizontal and vertical position of the holes and number of holes), but the method fails in obtaining it. To evaluate the performance of this methodology, we design an experiment where one of the individuals is removed from the database. Then we try to recreate it by using the inverse mapping of the LLE. In Fig. 4 we illustrate the original individual (on the left) along with the recovered one (on the right).

Comparing the original individual with the recovered one, we could conclude that the performance of this strategy is unsatisfactory. Indeed, it cannot reconstruct any of the original individuals. One of the aspects that may improve the methodology's performance is to add topological information to the strategy in order to obtain an appropriate clustering of the original database. As you can observe, the recovered individuals preserve the position of the holes in two scenarios (cases a and c) but never match the number of holes. Presumably, this behaviour is due to the reduced amount of information (small data). Therefore we propose to harness the available samples by extracting more information, i.e. the topology.

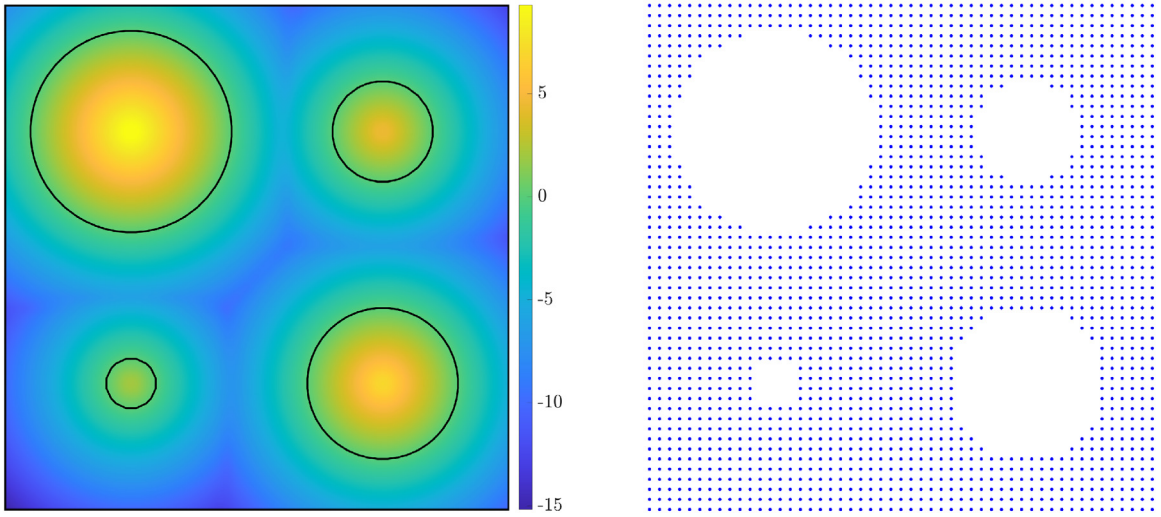

(a) Geometry descriptor of an individual composed by 4 circles.

(b) Equivalent point cloud.

Fig. 5. Synthetic example for TDA (a) SDF (zero value corresponds to the boundary, in black) (b) the resulting points employed for the TDA tools.

2.3. Geometry and topology-based strategy

This section revisits the conclusions gathered in the previous section and develops a strategy to possibly improve the overall performance of the previous one. The first modification considered consists in the addition of topological information. This section explains how topology is characterised, how this information is obtained and how we propose to merge geometrical and topological information. The final objective is to cluster the data into its different topologies to aid the interpolation scheme to create pertinent individuals.

2.3.1. Topological data analysis overview

In this work, we consider that the number of holes defines the topology of an object, so we need a tool to automatically infer the number of holes and give some sense of its size, but we also need to define a technique to properly compare different topologies. We propose to employ the Topological Data Analysis (TDA) [6,7] that encompasses a set of tools from high-dimensional data analysis which extract topological information from a group of points. These techniques are directly applicable as any SDF can be converted into a cloud of points employing the coordinates on the nodes in a Cartesian grid and its function value. The topological characterisation we use is based on the principle of persistent homology [5], which extracts the most relevant features in a point cloud; as mentioned, these features may be the number of holes and a sense of its size, for instance. In Fig. 5(a) we show an synthetic example of a component's SDF, along with its boundary, while, in Fig. 5(b), we represent the resulting set of points considered for the TDA strategy, i.e. negative values of the SDF represent the domain of the geometry.

Considering the resulting unconnected set of points $\in \mathbb{R}^2$, we define a circle with a radius r from each point. As the value of r increases, the connectivity of points changes. A connection is established when two or more points are inside of a circle of radius r. This change in connectivity allows the creation of geometrical entities such as edges or triangles, whose vertices are the set of points. At some moment, the connectivity of the points will create a set of edges that form a closed polygon. If we keep increasing r, the connectivity will create entities of higher dimensions, such as triangles that will cover the hole and then disappear. Persistent features detected with a wide range of spatial scales r are considered more likely to represent a true topological feature of the underlying point cloud instead of artefacts of the sampling or noise. The value r in which a persistent feature appears and disappears is used to create the persistence diagram (PD), representing the birth x and death y of each topological feature

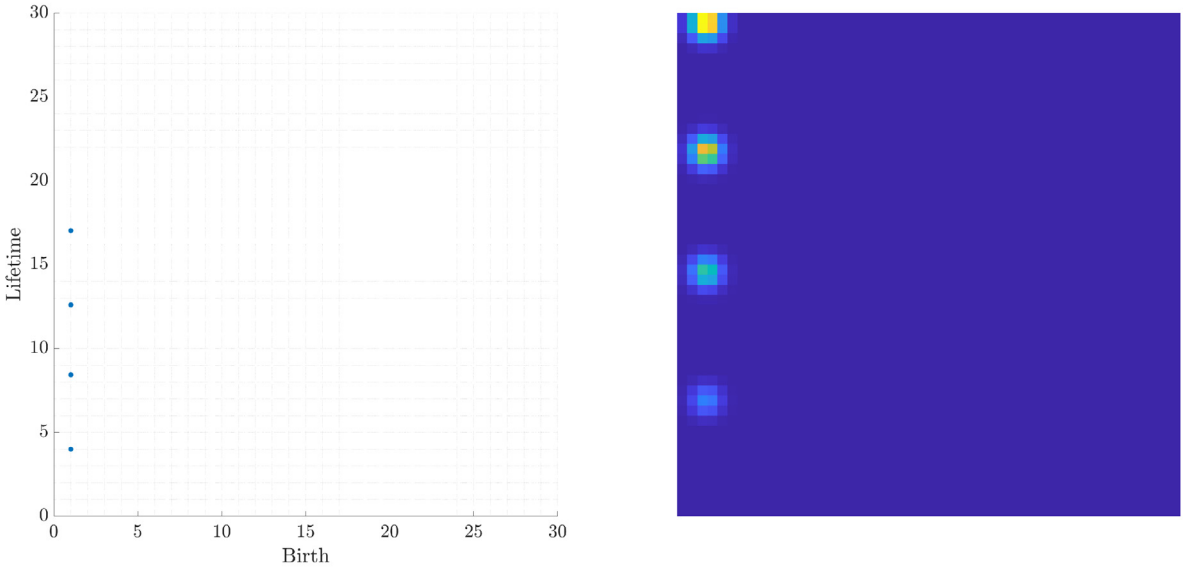

(a) Lifetime diagram. (b) Persistence image.

Fig. 6. Space transformation of the persistent homology from the lifetime diagram (a) to the persistence image (b).

found during the growth of r. As for any persistent feature, for instance, a hole, the birth precedes the death, all the points of the persistence diagram are located above the diagonal $y = x$, and any point (x, y) near the diagonal may represent noise or small scale features. Points far from the diagonal represent topological features that persist and may be considered to define the overall topology of the component.

The persistence diagram belongs to a non-metric space, so comparing or evaluating a distance between different persistence diagrams is not directly possible. Different representations of the persistent homology are available that contain the same information but are displayed differently. We obtain the lifetime diagram (LD) (see Fig. 6(a)) if we apply the mapping $f : (x, y) \rightarrow (x, y - x)$ to the persistence diagram (PD), as in the PD, points far from the x-axis represent more relevant topological features. The drawback of using those spaces is that they are not equipped with a norm, such as the L_2 metric commonly used in most Machine Learning applications. Thus, we need to apply space transformation to the current descriptor of topological features to a more appropriate representation equipped with a suitable norm. For that purpose, following the rationale in [8], we use the persistence surface, which is based on a Gaussian kernel evaluated in the space of the LD. The surface created is then reduced to a finite-dimensional discretised space. In particular, we fix a grid in the plane with $n \times n$ subdomains (pixels). The integration of the persistence surface over each pixel gives, as a result, the so-called Persistence Image (PI) $\in \mathbb{R}^2$ (see Fig. 6(b)) [8].

In Fig. 6(a), we illustrate how the four holes that appear in 5(b) are translated into the persistence diagram employing the persistent homology. Fig. 6(a) represents one point per hole, and its coordinates correspond to the value of r when the hole is detected in $x - axis$ and the total lifetime of the hole in $y - axis$. Notice that the birth of each feature is the same due to the uniformity of the grid used to describe the SDF. Fig. 6(b) illustrates the resulting persistence image obtained from the space transformation of the persistence diagram.

2.3.2. Modifications in LLE to consider geometry and topology

The modification of the original strategy considers adding the persistence image ($\mathbf{T}_i$) of each individual to its geometrical description defined by its SDF ($\mathbf{X}_i$) as the topological descriptor into the manifold learning stage. So far, the information to feed the LLE algorithm corresponded to the geometrical representation of the components, i.e., the SDF. To feed the LLE algorithm with both geometrical and topological information we propose to make use of a weighted linear combination of the distances from each shape descriptor, topological and geometrical, as,

$$d_{ij}^2 = \frac{\theta}{\sum_i \sum_j \|\mathbf{X}_i - \mathbf{X}_j\|^2} \cdot \|\mathbf{X}_i - \mathbf{X}_j\|^2 + \frac{(1-\theta)}{\sum_i \sum_j \|\mathbf{T}_i - \mathbf{T}_j\|^2} \cdot \|\mathbf{T}_i - \mathbf{T}_j\|^2 \tag{8}$$

where θ is the weighting factor.

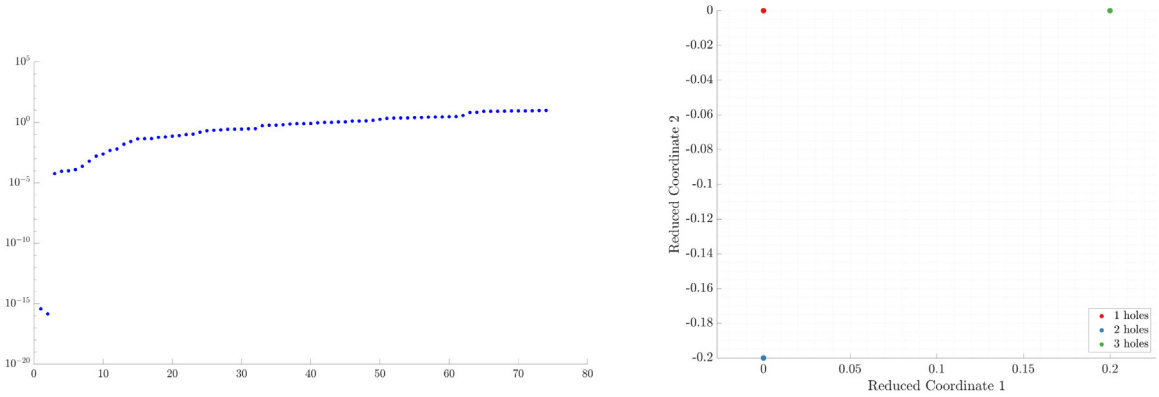

(a) Eigenvalue distribution.

(b) Two first coordinates of the reduced latent space.

Fig. 7. Resulting eigenvalue distribution (a) and reduced coordinates (b) by using the LLE technique including both, the original data and the persistence images.

Additionally, we introduce the topological information in the LLE by modifying Eq. (3), leading to:

$$\varepsilon(\mathbf{w}) = \sum_i \left[\frac{\theta}{\sum_i \sum_j \|\mathbf{X}_i - \mathbf{X}_j\|^2} \cdot \|\mathbf{X}_i - \sum_j^k w_{ij}\mathbf{X}_j\|^2 + \frac{(1-\theta)}{\sum_i \sum_j \|\mathbf{T}_i - \mathbf{T}_j\|^2} \cdot \|\mathbf{T}_i - \sum_j^k w_{ij}\mathbf{T}_j\|^2 \right], \tag{9}$$

where $\mathbf{X}_i$ is the level-set representation of the geometry, i.e., the SDF and $\mathbf{T}_i$ is the corresponding persistence image. The optimal $\mathbf{w}$ takes into account a mixture of the likeness of the geometry and topology.

2.3.2.1. Weighting factor selection. Considering the previously discussed modifications of the standard LLE implementation and the reference database, we compute the local vicinities of each individual considering the distance defined in Eq. (8). Later, we continue with the minimisation of the functional in Eq. (9). The next steps of the algorithm LLE are not modified. As in the previous example, we consider $k = 4$ neighbours with a randomly defined weighting factor of $\theta = 0.5$. In Fig. 7(a) we show the distribution of the eigenvalues obtained from the LLE, and we conclude that the reduced dimensions are 2, again failing in obtaining the right number of dimensions. Fig. 7(b) illustrates the projection of each individual to the reduced manifold of two dimensions.

Here we see that each cluster is collapsed in one point in the reduced manifold, which prevents the extraction of geometrical modes, as well as the interpolation between individuals, indicating, perhaps that the topology information has too much influence. Hence, we modify the value of the weighting factor, in this case, $\theta = 0.8$. As in the previous example, Fig. 8(a) shows the eigenvalues obtained, which suggests us that 3 reduced dimensions seem acceptable, as expected, in this case. In Fig. 8(b) we also represent the spatial distribution of the projected individuals in the reduced manifold.

With this value of the weighting factor θ, we improve the clusterisation with respect to the previous example. We could also extract geometrical information related to the horizontal and vertical location of the circles, which was impossible considering the previous value of the weighting factor θ.

As in the previous experiment, we evaluate the method's performance trying to recover several individuals removed from the dataset. Fig. 9 shows the comparison between the original individual and the recovered one using the expression shown in (1). Even though the clusterisation is drastically improved, the recovered functions are far from the original ones, they match the position of the holes and slightly the topology but the results are not satisfactory so far. At this moment, our hypothesis here is that we have been able to properly organise the dataset in the reduced space, but that we lack of a proper interpolation approach to define the manifold.

The influence of the weighting factor may be seen as a regularisation in the metric. This regularisation enables the modification of the quantity of topological information added to the metric. However, the weighting factor is a hyperparameter and must be set by the user. The fulfilment of some criterion may guide the selection of its value. Different criteria may be considered, such as seeking a particular characteristic in the reduced manifold, for instance, the clusterization in topologies, or improving the quality of the recovered individuals.

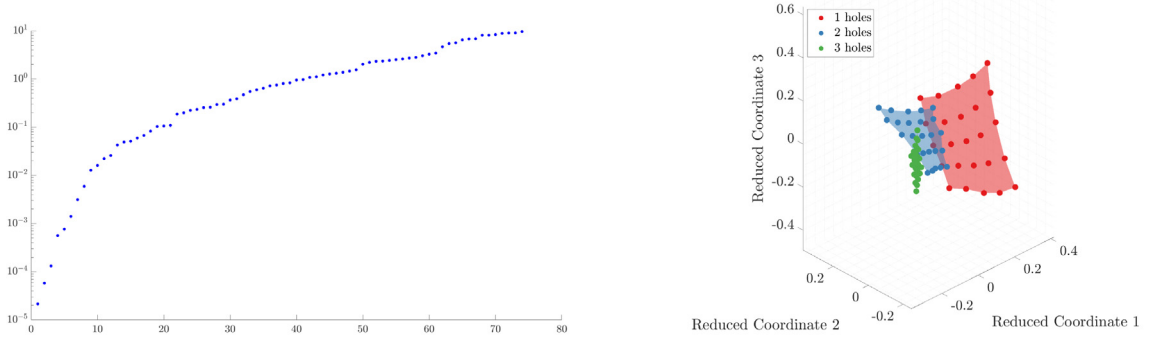

(a) Eigenvalue distribution. (b) Three first coordinates of the reduced latent space.

Fig. 8. Resulting eigenvalue distribution (a) and reduced coordinates (b) by using the LLE technique considering the original data and the persistence images.

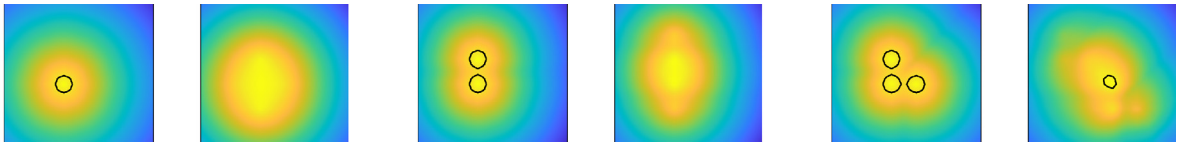

(a) Original component with one holes (left) and the recovered one (right). (b) Original component with two holes (left) and the recovered one (right). (c) Original component with three holes (left) and the recovered one (right).

Fig. 9. Examples of original components removed from the database and the recovered ones by the vicinity information.

2.3.3. *Optimal transport-based interpolation to recover dimensionality*

A relevant characteristic of the LLE is that it allows to define one individual through the linear interpolation between the neighbours of its vicinity (1). Due to the scarcity of data this interpolation scheme, considering the original LLE technique is not appropriate, as seen before. This is why we propose to rely on an Optimal Transport approach for the objects' interpolation [21–24].

2.3.3.1. Optimal transport overview. Optimal Transport techniques are based on the use of the Wasserstein distance W_2 between objects, also known as Earth Mover's distance [22,23]. These distances represent the geometric likeness between two objects by measuring the minimal amount of "work" needed to move the mass contained in one object onto the other. We may extrapolate this capability to tasks like geometric domain interpolation by solving the barycentre problem [25] stated as,

$$\mathbf{Z}_i^* = \arg\min_{\mathbf{Z}_i} \sum_{j=1}^{k} w_j W_2^2(\mathbf{Z}_i, \mathbf{Z}_j). \tag{10}$$

where, $\mathbf{Z}_i$ and $\mathbf{Z}_j$ correspond to the interpolated individuals and the individuals used for the interpolation, respectively. Also, W_2 corresponds to the Wasserstein metric and w_j are the interpolation weights. In Fig. 10 we illustrate the resulting functions obtained from the linear and the optimal transport interpolation between two original functions.

2.3.3.2. Applying optimal transport-based interpolation to the reference database. As seen in Section 2.3.3.1 the improvements achieved in the clustering task were not translated to the recovery performance. Considering the manifold obtained in Fig. 8(b), we modify the interpolation scheme, in this case, using the tools from OT. In Fig. 11, we solve the barycentre problem considering the Wasserstein distance after transforming the original SDF into a probabilistic function which indicates the probability that a point is inside the geometry, being the implicit boundary described by the 0.5 value. Fig. 11 shows that the original components and the recovered ones are virtually

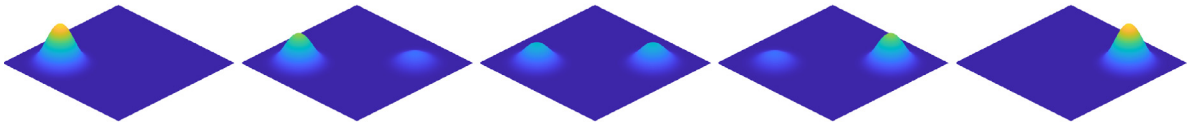

(a) Linear interpolation

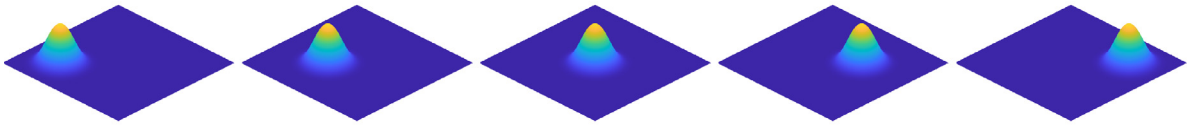

(b) Optimal Transport interpolation

Fig. 10. Comparison between linear and optimal transport interpolation. Figures on left and right are the original functions while the middle figures show their weighted interpolation.

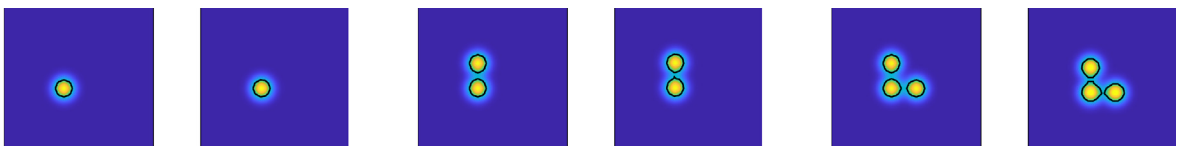

(a) Original component with one holes (left) and the recovered one (right).

(b) Original component with two holes (left) and the recovered one (right).

(c) Original component with three holes (left) and the recovered one (right).

Fig. 11. Examples of original components removed from the database and the recovered ones by the vicinity information.

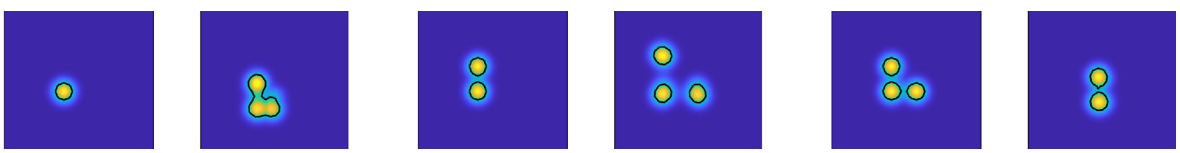

(a) Original component with one holes (left) and the recovered one (right).

(b) Original component with two holes (left) and the recovered one (right).

(c) Original component with three holes (left) and the recovered one (right).

Fig. 12. Examples of original components removed from the database and the recovered ones by the vicinity information, considering the OT strategy but not taking into account topology information.

the same; thus, the modification in the interpolation scheme entail a relevant improvement in the reconstruction of objects.

It is interesting to get insight of the relative effect of optimal transport and the use of topological descriptors. For this, we apply the OT strategy without adding topological information (manifold shown in Fig. 3(b)). This change the set of neighbours used to reconstruct individuals. From Fig. 12 we can see that an OT strategy associated with a poor clustering does not lead to satisfactory results. Hence, from now on, in this paper we will rely on the simultaneous use of both strategies.

3. Numerical example

This section shows how the previous methodology is applied to an industrial example that mimics car's bumpers. Due to the impossibility of gathering actual data, we create the database artificially through a hybrid optimisation technique [20,32]. We have generated a database that simulates the work of manufacturers, specifically those engaged in the car's bumper design. This example tries to mimic the actual designs of a car's bumper considering a simplified 2D domain. The design domain of the problem (see Fig. 13) is characterised by variables h_1, h_2, and X, which define the region where the material is allowed to exist. The Dirichlet boundary conditions are defined by the variables w and W, that specify the position where all displacements are restricted. Additionally, the variable

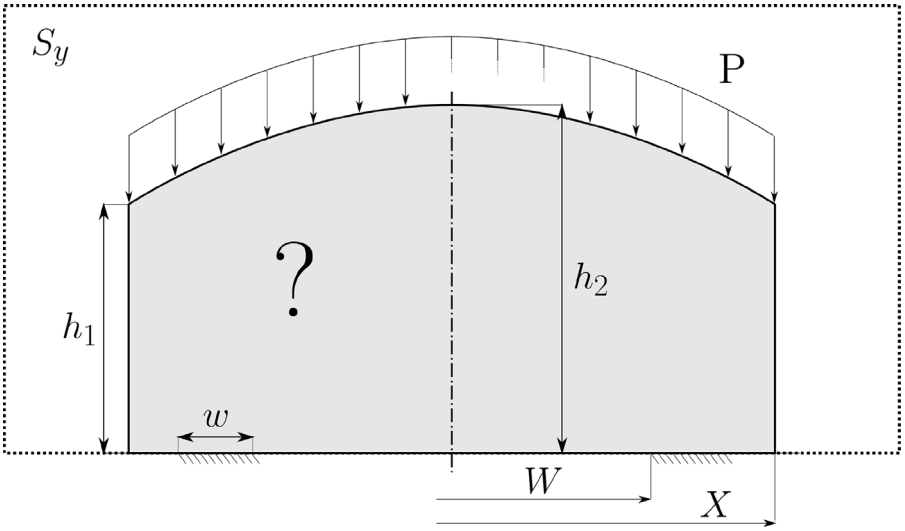

Fig. 13. Parametrisation of the variables that define the design domain and the boundary conditions of the hybrid optimisation algorithm.

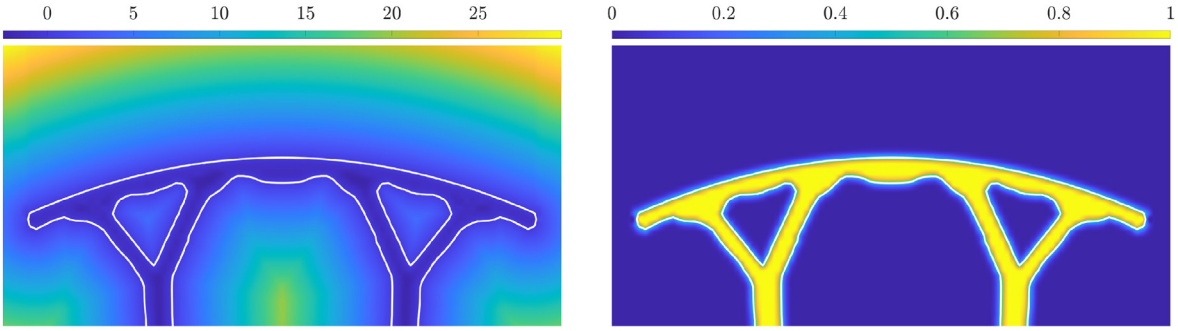

(a) Geometry defined by a SDF.

(b) Geometry defined by a probabilistic function.

Fig. 14. Conversion of the SDF (a) into a probabilistic distribution (b).

P determines the value of the pressure applied; for all bumpers, we define the value of P in order to get the same resulting force applied to each bumper. This problem shows how the presented strategy works with more complex examples where the scarcity of data is also considered.

Fig. 14(a) shows an example of the resulting component obtained through the hybrid optimisation algorithm. This figure represents the SDF, with the boundary defined by its zero value. However, the input geometrical objects must be described by a probabilistic function to use the OT tools properly. In our case, we convert the SDF into a probabilistic function with its limits between 0 and 1 and the boundary described using the mid-value, 0.5. The value of the probabilistic function indicates the probability that a point belongs to the interior of the geometry, which, for a given kernel, is straightforward when the SDF is available. Then, Fig. 14(b) illustrates the resulting function that describes the geometry of the component after its transformation.

Fig. 15 shows a representative sampling of 9 individuals the database, which is composed of 83 individuals. Also, each individual is discretised by 10,201 nodes. From now on, the standard geometrical descriptor will be the probabilistic function for representation purposes. Even though bumpers conform to the original dataset with various topologies, we neglect those with little importance. Then, the final database, as illustrated in Fig. 15 consists of bumpers whose topology has 2 holes or none of them, as only a very reduced number of bumpers with more than 2 holes were obtained during the creation of the database.

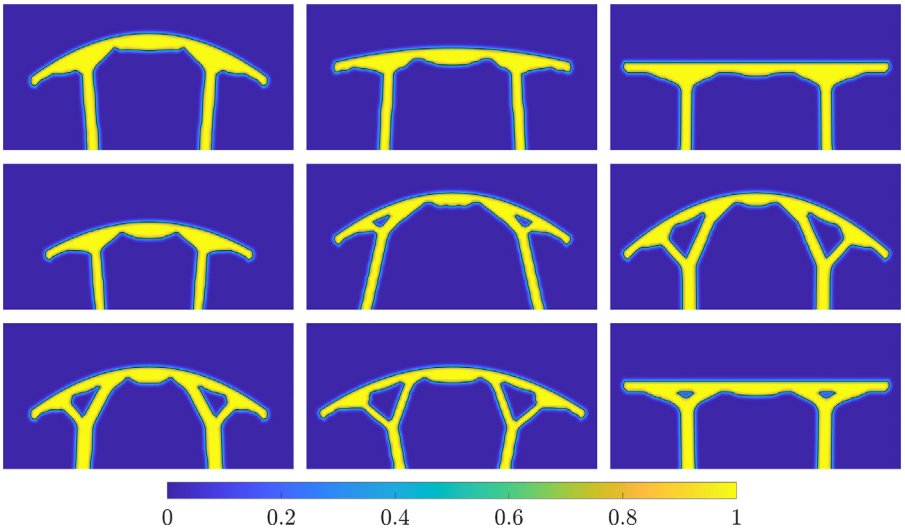

Fig. 15. Probabilistic functions of sampled components from the database.

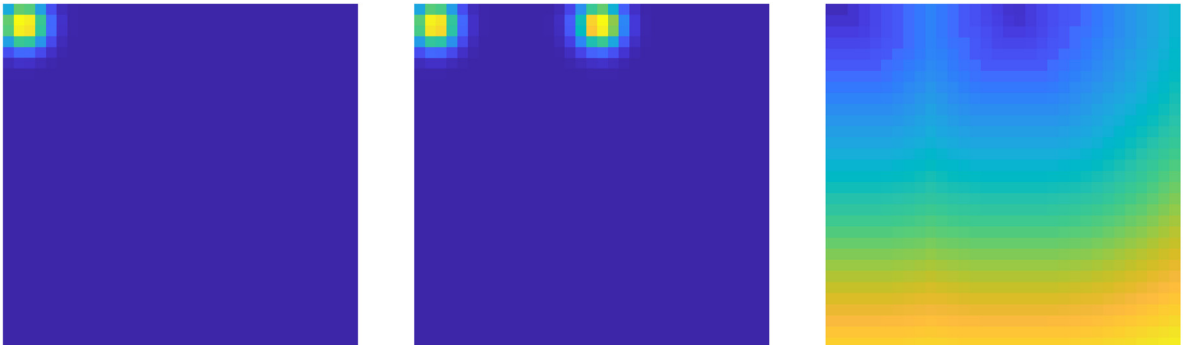

(a) Persistence diagram. (b) Modified persistence diagram. (c) Level-set function over the modified persistence diagram.

Fig. 16. Persistent homology of the car's bumper in Fig. 14 considering the repeatability of each persistent feature.

3.1. Topological characterisation

As a reminder, the final proposed strategy considers the complete characterisation of the shape of a component, including its geometry and topology. Thus, the next step is to obtain the persistent homology of each bumper in the database. Let us consider the bumper in Fig. 14(b), which presents two holes, to better illustrate the topological characterisation. We would compute the persistence image of each individual employing its persistent homology. The persistent homology, in this example (see Fig. 16(a)), seems to capture one of the two holes, which may indicate that they are overlapped in the representation as the birth and lifetime are the same. This behaviour may be a source of issues in the clustering task, so we consider a different coordinate system to represent the persistent homology. As the we use a uniform grid to represent the probabilistic function of each bumper, the birth of each hole is always the same (the spacing of the grid), so we assume that this coordinate its not that relevant and consider a different coordinate that includes the times a identical topological feature is repeated. So, the *x-axis* of the lifetime diagram, previously representing the birth, is replaced by the repeatability coordinate, providing the corresponding persistence image in Fig. 16(b), where two holes are now represented. As most of the image domain has 0 value, this image may be converted into a function over the whole domain, for instance, employing the level-set method (see Fig. 16(c)).

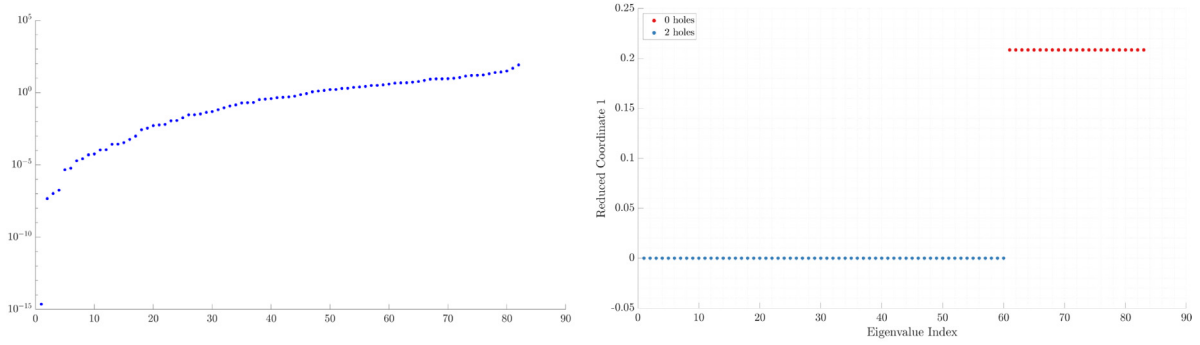

(a) Eigenvalue distribution. (b) First coordinate of the reduced latent space.

Fig. 17. Resulting eigenvalue distribution (a) and reduced coordinates (b) by using the LLE technique with the original data plus the persistence images.

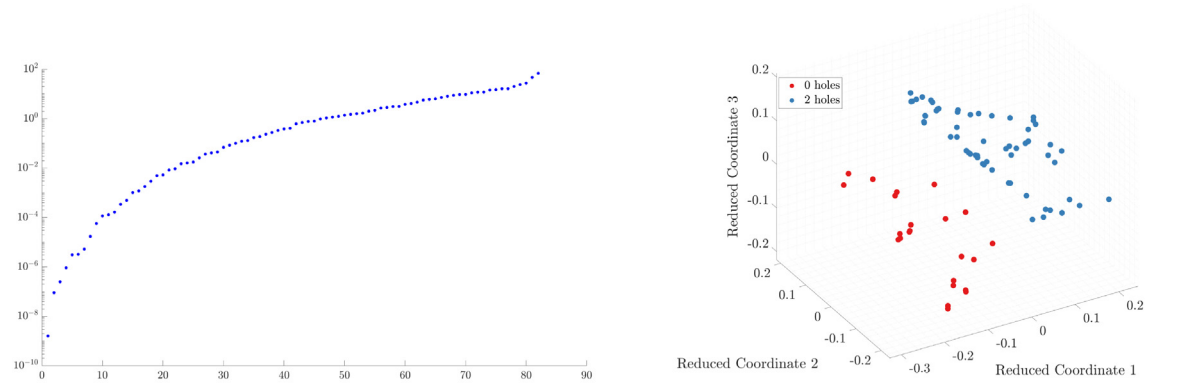

(a) Eigenvalue distribution. (b) Three first coordinates of the reduced latent space.

Fig. 18. Resulting eigenvalue distribution (a) and reduced coordinates (b) by using the LLE technique with the original data plus the persistence images.

3.2. Influence of the weighting factor θ

Once the database has been processed, we have two shape descriptors for each component: a geometrical descriptor defined as a probabilistic function and a topological descriptor described with the persistence image. The next step within the proposed strategy consists in obtaining the reduced manifold containing the projection of each individual. For this problem, we used the modified version of the LLE that merges geometrical and topological information and use the euclidean distance to evaluate the local vicinities as in Eq. (8). The value of the weighting factor is arbitrarily set to $\theta = 0.5$, and the vicinity is set to 9 neighbours. Fig. 17(a) shows the eigenvalue distribution, where the smallest one is far from the rest, which implies that there is one dominant dimension in the reduced manifold. This seems strange as it is difficult to represent properly all the geometrical and topological details we described above with just one dimension. That is why we decided to modify the value of the weighting factor. Indeed, Fig. 17(b) shows the representation of the components in the reduced manifold and we conclude that just the topology is inferred, so we must increase the contribution of the geometrical descriptor.

For the next test, we set the value of the weighting factor to $\theta = 0.7$. Fig. 18(a) shows the eigenvalue distribution where now more dimensions seem to characterise the database. In this example, we selected the 3 first dimensions, for representation purpose, as shown in Fig. 18(b), to describe the resulting reduced manifold. These results show that an appropriate selection of θ is required. In practice, the user should test several configurations of the hyperparameters θ and number of neighbours k until satisfied with the reduced space.

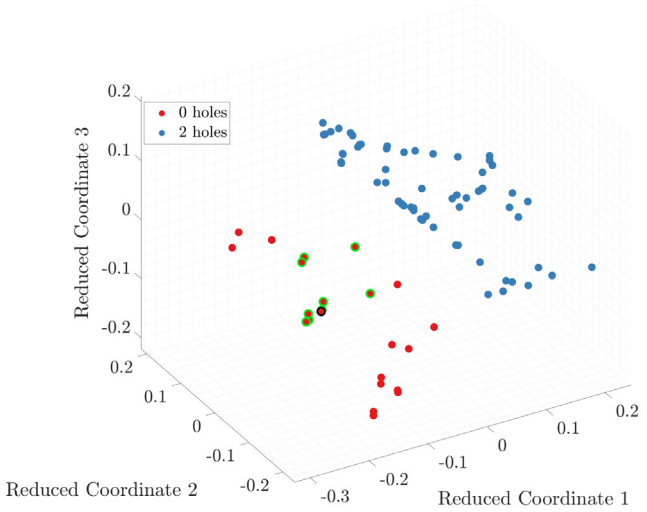

(a) Latent space where we highlight the reference individual (in black) and the neighbours used to recover it (in green).

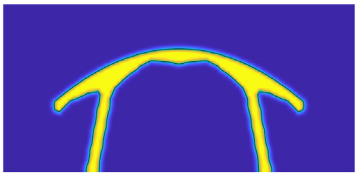

(b) Reference bumper.

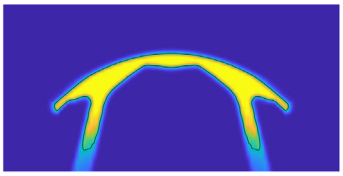

(c) Bumper recovered by linear interpolation.

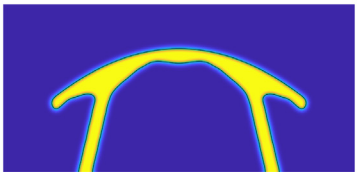

(d) Bumper recovered by optimal transport interpolation.

Fig. 19. Recovery of a bumper of the cluster with 0 holes removed from the database. (For interpretation of the references to colour in this figure legend, the reader is referred to the web version of this article.)

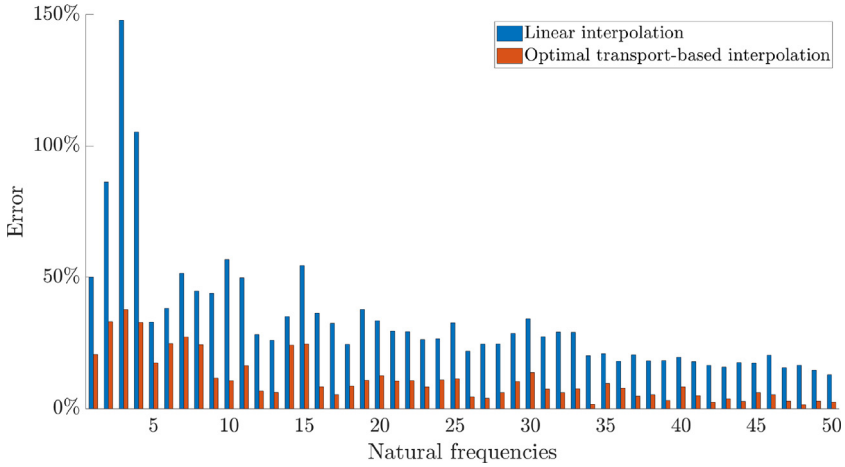

Fig. 20. Error measure of each natural frequency for the reconstruction employing the linear interpolation (blue) and the optimal transport-based interpolation (orange).

3.3. Results

To check the feasibility of this methodology to produce components with physical sense and framed on the nature of the database, we repeat the same experiment as done with the moving circles example. This experiment consists of removing an individual from the database and trying to recover it using the inverse mapping of the LLE proposed in this paper. Figs. 19 and 21 show examples of recovered individuals. Each Figure shows the recovery of one random individual selected from each of the clusters (cluster of topologies with 0 holes in Fig. 19 and with 2 holes in Fig. 21). In each case, we present, using probabilistic functions, the original geometry to be recovered and the results obtained through linear interpolation and with the proposed strategy that computes the barycentre problem considering the

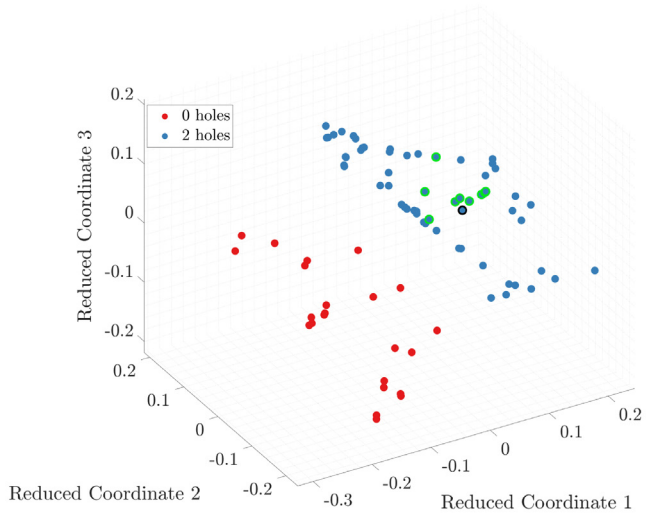

(a) Latent space where we highlight the reference individual (in black) and the neighbours used to recover it (in green).

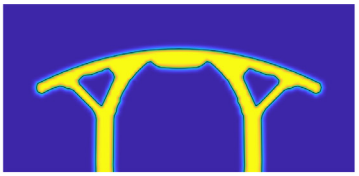

(b) Reference bumper.

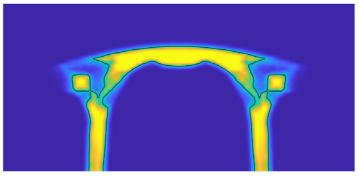

(c) Recovered bumper by linear interpolation.

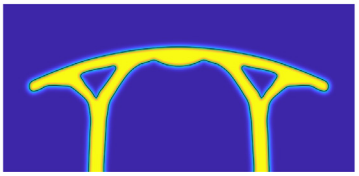

(d) Recovered bumper by optimal transport interpolation.

Fig. 21. Recovery of a bumper of the cluster with 2 holes removed from the database. (For interpretation of the references to colour in this figure legend, the reader is referred to the web version of this article.)

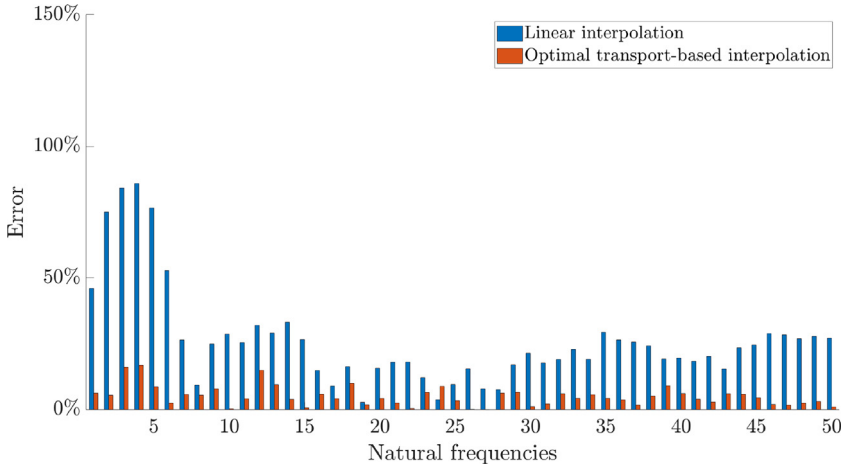

Fig. 22. Error measure of each natural frequency for the reconstruction employing the linear interpolation (blue) and the optimal transport-based interpolation (orange).

Wasserstein distances. Some individuals are highlighted in these figures: the reference bumpers to be recovered, removed from the database, (highlighted with a black contour) and the neighbours used to recover the reference bumper (highlighted with a green contour). Analysing the recovered components, we conclude that the interpolation based on OT techniques provides components with physical sense, quite similar to the reference component and preserving the features in the database, while, on the contrary linear-based interpolation schemes seem to produce bumpers with artefacts and loss of features, that, consequently will prevent any successful numerical simulation. Additionally to the qualitative comparison in Figs. 19 and 21, we compute a quantitative difference between the recovered bumpers and the reference one. As this component will fulfil certain structural criteria, we consider it interesting to compute an error metric based on its structural behaviour. Therefore, we carry out a modal analysis

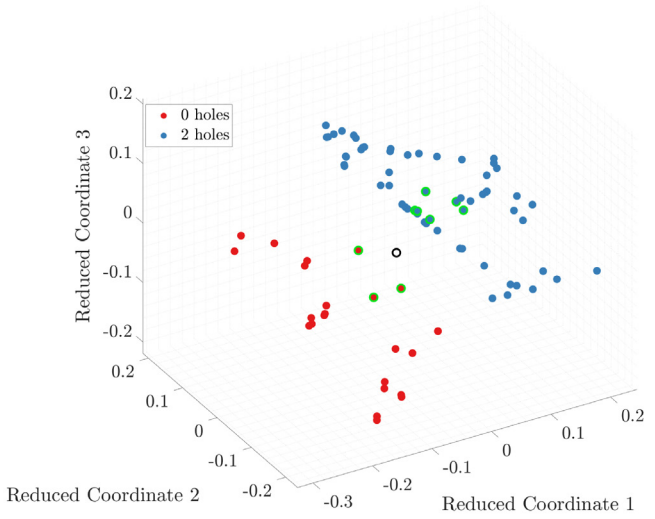

(a) Latent space where we highlight the reference individual (in black) and the neighbours used to recover it (in green).

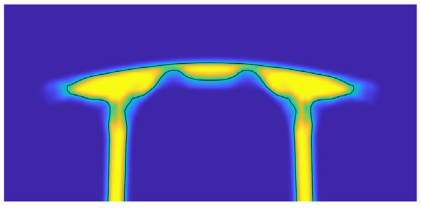

(b) Recovered bumper using linear interpolation.

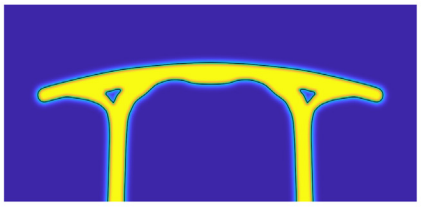

(c) Recovered bumper using optimal transport interpolation.

Fig. 23. Creation of a new bumper employing the proposed methodology. (For interpretation of the references to colour in this figure legend, the reader is referred to the web version of this article.)

in each recovered component and then, we compare its first natural frequencies (removing those associated with the rigid solid movement) considering the following expression to measure its error,

$$Error_i = 100 \cdot \left| \frac{\hat{\omega}_i - \omega_i}{\omega_i} \right|, \tag{11}$$

where, $\hat{\omega}_i$ and ω_i correspond to the ith natural frequency of the recovered bumper and the reference one, respectively. The error of the example in Fig. 19 is illustrated in 20, while Fig. 22 represents the error of the example pictured in Fig. 19. In general terms, both Figures show that the bumper obtained employing the optimal transport-based interpolation presents lower error levels for the first 50 natural frequencies.

With the creation of the reduced manifold, we are not limited to recover individuals in the database. Instead we are also able to navigate along this manifold being able to obtain the projection of the original high dimensional space corresponding to the points on the low dimensional manifold. The resulting projection of these points will entail the creation of new components non-existing in the original database, as we will be able to retrieve the geometrical and topological information. Fig. 23(a) shows an arbitrary point in the reduced manifold located between the topological clusters, along with the neighbours, of different topologies, used for its interpolation. Figs. 23(b) and 23(c) illustrate the resulting component obtained by linear and by optimal transport interpolations.

In order to illustrate the robustness and the generative capability of the methodology proposed, we extend this numerical example by adding a new experiment. Based on the previous example (Fig. 23), this experiment navigates within the manifold and generates new bumpers that are non-existing in the original database. We use the bumper coordinates in Fig. 23 as a reference. Then we define 3 directions, each corresponding to the axis of the coordinate system of the reduced parametric space. As a reminder, we use the LLE technique that extracts the non-linear structure of the high-dimensional data. In our example, these are a set of non-linear geometrical modes. The non-linearity means that each mode may influence the recovered data differently depending on its position in the manifold. Therefore, this experiment shows the local influence of each axis in the neighbourhood of the reference coordinates. Generally, we can conclude that the first dimension is in charge of the bumper's curvature. In contrast, the second one seems more related to the topological change and the holes' size. Finally, the third one may modify the bumper's overall height and the holes' size. Fig. 24 illustrate this experiment where the reduced manifold along with the points of the study are represented in Fig. 24(a). Also, Figs. 24(b)–24(d) show the resulting set of bumpers in each axis. Not all bumpers have the structural qualities we might expect, for instance, the first bumper of the second axis. It seems that this is a region where the topology of the bumper changes. The holes

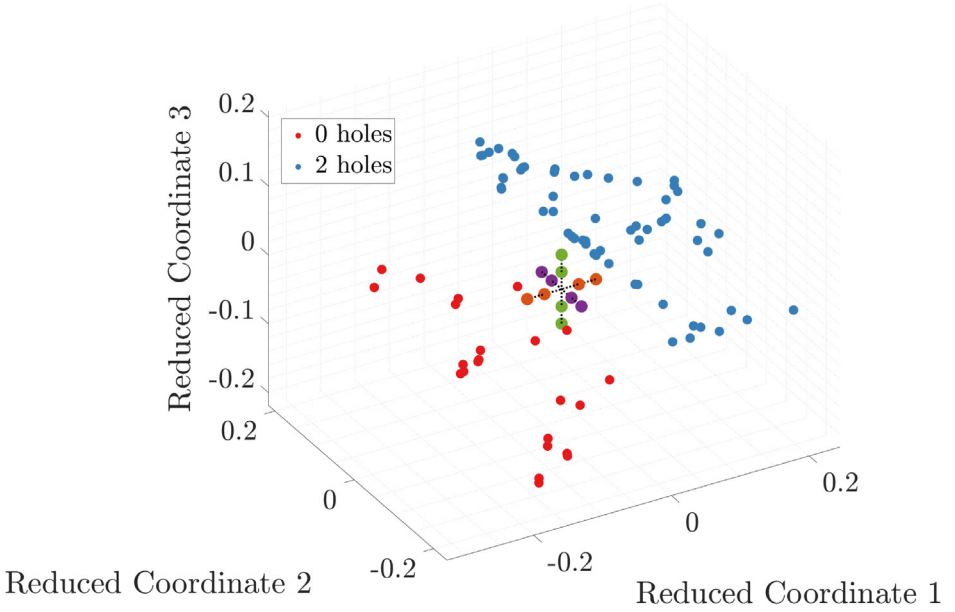

(a) Latent space where we highlight the query points, classified by the variation in its coordinates: reduced dimension 1 (orange points), reduced dimension 2 (purple points) and reduced dimension 3 (green points).

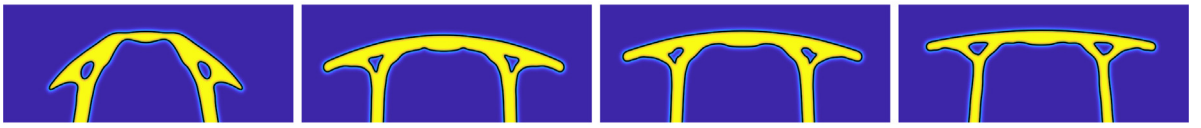

(b) Evolution of individuals according to the reduced dimension 1 (orange points).

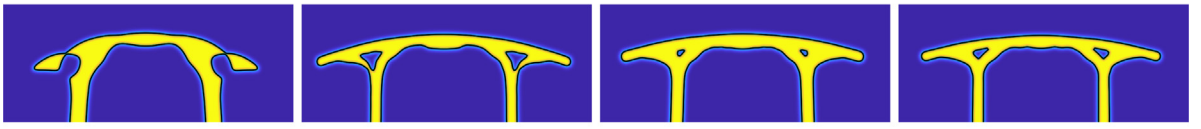

(c) Evolution of individuals according to the reduced dimension 2 (purple points).

(d) Evolution of individuals according to the reduced dimension 3 (green points).

Fig. 24. Creation of a set of new bumpers employing the proposed methodology. (For interpretation of the references to colour in this figure legend, the reader is referred to the web version of this article.)

in the component get bigger until they reach the surface, therefore, modifying the topology. However, we can still extract some conclusions about the influence of each axis on the characteristic of the generated bumper.

4. Conclusions

We have proposed a strategy to create a low dimensional manifold to describe an existing database of designs defined by their geometry and topology. We are able to navigate within this manifold not only to recover existing designs but, more interesting, to create new coherent designs. We have accomplished this goal using different tools such as the LLE, the TDA and the OT. To conclude the current work, we would like to synthesise some final thoughts:

- Manifold Learning (ML) strategies, such as the Locally Linear Embedding, are appropriate tools to visualise and manipulate high-dimensional data by extracting the inherent latent structure. The resulting dimensions may be considered a shape generator basis, employing the inverse mapping to recover the original dimensionality.
- The use of the level-set method seems to be a coherent framework to characterise the geometry of the components as it allows direct comparison between different shapes. We found the widely used Signed Distance Functions convenient for our purposes.
- Topological Data Analysis tools aid the clustering task carried out by the dimensionality reduction algorithm.
- We propose to adequately combine the geometrical description provided by the SDFs with topological information to obtain a synergetic effect. This requires the definition of θ, a parameter that weights the influence of these two different informations.
- The use of Optimal Transport tools in the ML strategy represents a definitive improvement with respect to the standard LLE algorithm implementation. Thanks to these techniques, the recovered individuals resemble the original database and have a physical sense from a structural point of view.
- Due to the computational cost of evaluating the Wasserstein distances, we propose a compromise strategy, where the Wasserstein distances are computed just when interpolating, instead of using them to create the reduced space.
- In the same way, using the LLE, allows to evaluate the Wasserstein distances among few neighbours instead of the full database.
- One of the limitations of the proposed methodology is its maturity. We still need to establish a metric that assesses the quality of the component reconstruction for any problem. For this reason, we cannot measure the influence of each hyperparameter appearing in the methodology, like the weighting factor or the number of neighbours, possibly leading to reduced manifolds not being able to extract the knowledge of the database.
- Once these limitations are surpassed, the potential applications of the methodology are several. For instance, it could be used for the development of a design tool able to propose, taking the know-how into account, predesigns characterised by the sets of parameters defined by the user. These predesigns may be then modified to meet other design requirements. Also, this methodology could be used for the development of an optimisation algorithm that navigates the resulting reduced manifold to find the optimal component that maximises/minimises an objective function subject to a set of design constraints.

5. Future works

In this last section we would like to highlight some future developments from the current work:

- As we show with the last example, we are able to navigate the reduced manifold to obtain new components non-existing in the original dataset. This tools could be used, for instance, to obtain components defined in terms of geometrical and/or topological constraints or in terms of the structural behaviour of the component, for example.
- The selection of the weighting factor θ may be guided by and optimisation algorithm by looking for some specific characteristics of the resulting reduced manifold.

Declaration of competing interest

The authors declare that they have no known competing financial interests or personal relationships that could have appeared to influence the work reported in this paper.

Data availability

Data will be made available on request.

Acknowledgements

The authors gratefully acknowledge the financial support of Ministerio de Educación, Spain (FPU16/07121), Generalitat Valenciana, Spain (Prometeo/2021/046 and CIAICO/2021/226), Ministerio de Economía, Industria *y* Competitividad, Spain (DPI2017-89816-R) and FEDER. O. Allix would like to thank the French National University Council and ENS Paris-Saclay for supporting his sabbatical at UPV, which made it possible to closely interact with the colleagues from I2MB-UPV. Funding for open access charge: CRUE-Universitat Politècnica de València

References

[1] UNIDO, Manual on Technology Transfer Negotiation, in: General Studies Series, Vienna, 1996.
[2] A. Krizhevsky, I. Sutskever, G.E. Hinton, ImageNet classification with deep convolutional neural networks, Commun. ACM 60 (6) (2017) 84–90.
[3] R. Malladi, J.A. Sethian, B.C. Vemuri, Shape modeling with front propagation: A level set approach, IEEE Trans. Pattern Anal. Mach. Intell. 17 (2) (1995) 158–175.
[4] T. Chan, W. Zhu, Level set based shape prior segmentation, in: Proceedings - 2005 IEEE Computer Society Conference on Computer Vision and Pattern Recognition, Vol. II, CVPR 2005, IEEE Computer Society, 2005, pp. 1164–1170.
[5] A. Zomorodian, G. Carlsson, Computing persistent homology, Discrete Comput. Geom. 33 (2) (2005) 249–274.
[6] G. Carlsson, Topology and data, Bull. Amer. Math. Soc. 46 (2) (2009) 255–308.
[7] L. Wasserman, Topological data analysis, Annu. Rev. Stat. Appl. 5 (2018) 501–532.
[8] H. Adams, T. Emerson, M. Kirby, R. Neville, C. Peterson, P. Shipman, S. Chepushtanova, E. Hanson, F. Motta, L. Ziegelmeier, Persistence images: A stable vector representation of persistent homology, J. Mach. Learn. Res. 18 (2017) 1–35.
[9] I.T. Jolliffe, Principal Component Analysis, second ed., in: Springer Series in Statistics, vol. 98, 2002, p. 487.
[10] J.W. Sammon, A nonlinear mapping for data structure analysis, IEEE Trans. Comput. C-18 (5) (1969) 401–409.
[11] B. Schölkopf, A. Smola, K.R. Müller, Nonlinear component analysis as a Kernel eigenvalue problem, Neural Comput. 10 (5) (1998) 1299–1319.
[12] M. Belkin, P. Niyogi, Laplacian eigenmaps for dimensionality reduction and data representation, Neural Comput. 15 (6) (2003) 1373–1396.
[13] J.B. Tenenbaum, V. De Silva, J.C. Langford, A global geometric framework for nonlinear dimensionality reduction, Science 290 (5500) (2000) 2319–2323.
[14] M.A. Kramer, Nonlinear principal component analysis using autoassociative neural networks, AIChE J. 37 (2) (1991) 233–243.
[15] P. Vincent, H. Larochelle, I. Lajoie, Y. Bengio, P.A. Manzagol, Stacked denoising autoencoders: Learning useful representations in a deep network with a local denoising criterion, J. Mach. Learn. Res. 11 (2010) 3371–3408.
[16] D.P. Kingma, M. Welling, An introduction to variational autoencoders, Found. Trends Mach. Learn. 12 (4) (2019) 307–392.
[17] S.T. Roweis, L.K. Saul, Nonlinear dimensionality reduction by locally linear embedding, Science 290 (5500) (2000) 2323–2326.
[18] D. González, E. Cueto, F. Chinesta, Computational patient avatars for surgery planning, Ann. Biomed. Eng. 44 (1) (2016) 35–45.
[19] E. Nadal, D. Muñoz, N. Vivó, I. Lucas, J.J. Ródenas, Evaluation of hip fracture risk using a hyper-parametric model based on the locally linear embedding technique, C. R. Acad. Sci. 347 (11) (2019) 856–862.
[20] D. Muñoz, E. Nadal, J. Albelda, F. Chinesta, J. Ródenas, Allying topology and shape optimization through machine learning algorithms, Finite Elem. Anal. Des. 204 (2022) 103719.
[21] F.L. Hitchcock, The distribution of a product from several sources to numerous localities, J. Math. Phys. 20 (1–4) (1941) 224–230.
[22] L. Kantorovitch, On the translocation of masses, Manage. Sci. 5 (1) (1958) 1–4.
[23] L.V. Kantorovich, Mathematical methods of organizing and planning production, Manage. Sci. 6 (4) (1960) 366–422.
[24] C. Villani, Topics in optimal transportation, 2003, p. 390.
[25] J. Solomon, F. De Goes, G. Peyré, M. Cuturi, A. Butscher, A. Nguyen, T. Du, L. Guibas, Convolutional Wasserstein distances: Efficient optimal transportation on geometric domains, ACM Trans. Graph. 34 (4) (2015) 1–11.
[26] E. Burman, S. Claus, P. Hansbo, M.G. Larson, A. Massing, CutFEM: Discretizing geometry and partial differential equations, Internat. J. Numer. Methods Engrg. 104 (7) (2015) 472–501.
[27] J. Parvizian, A. Düster, E. Rank, Finite cell method : h- and p-extension for embedded domain problems in solid mechanics, Comput. Mech. 41 (1) (2007) 121–133.
[28] A. Düster, J. Parvizian, Z. Yang, E. Rank, The finite cell method for three-dimensional problems of solid mechanics, Comput. Methods Appl. Mech. Engrg. 197 (45–48) (2008) 3768–3782.
[29] D. Schillinger, M. Ruess, The finite cell method: A review in the context of higher-order structural analysis of CAD and image-based geometric models, Arch. Comput. Methods Eng. 22 (3) (2015) 391–455.
[30] J.J. Ródenas, O.A. González-Estrada, J.E. Tarancón, F.J. Fuenmayor, A recovery-type error estimator for the extended finite element method based on singular+smooth stress field splitting, Internat. J. Numer. Methods Engrg. 76 (4) (2008) 545–571.
[31] J.J. Ródenas, O.A. González-Estrada, P. Díez, F.J. Fuenmayor, Accurate recovery-based upper error bounds for the extended finite element framework, Comput. Methods Appl. Mech. Engrg. 199 (37–40) (2010) 2607–2621.
[32] D. Muñoz, J. Albelda, J.J. Ródenas, E. Nadal, Improvement in 3D topology optimization with h-adaptive refinement using the Cartesian grid finite element method, Internat. J. Numer. Methods Engrg. (2021).